A global Bayesian temperature calibration for lacustrine brGDGTs

Pablo Martínez-Sosa[a], Jessica E. Tierney[a], Ioana C. Stefanescu[b], Emily Dearing Crampton-Flood[d], Bryan N. Shuman[b], Cody Routson[c]

[a]*Department of Geosciences, The University of Arizona, 1040 E 4th St, Tucson, Arizona 85721, USA*
[b]*Department of Geology and Geophysics, University of Wyoming, Laramie, WY, USA*
[c]*School of Earth Sciences and Environmental Sustainability, Northern Arizona University, Arizona, USA*
[d]*School of Earth and Environmental Sciences, The University of Manchester, Manchester, UK*

Abstract

Despite widespread use of branched glycerol dialkyl glycerol tetraethers (brGDGTs) for paleo-temperature reconstruction, no global calibration for their application in lakes has been generated since improved analytical methods have allowed for the separation of the structural isomers. This is a substantial obstacle for the application of this tool as soil calibrations underestimate temperature values when applied to lake sediments. Here, we present a comprehensive dataset ($N = 272$) of lacustrine brGDGT distributions, consisting of both new and previously reported samples, spanning a wide range of geographical locations, environmental temperatures, and lakewater pH values. Empirical Orthogonal Function (EOF) analysis on the fractional abundance of brGDGTS indicates that temperature exerts a strong control (explaining 58% of the variance) on the lipid distribution. The influence of water chemistry is weaker, with pH and conductivity explaining 24% of the variance. We use our dataset to generate a new Bayesian temperature calibration, which has an $R^2 = 0.82$ and RMSE = 2.9°C. Application of the new temperature calibration to a previously published lake core record demonstrates that it generates values comparable to instrumental observations. Our new calibration facilitates the use of lacustrine brGDGTs to reconstruct continental temperatures, a vital piece of information for understanding past climates.

Preprint submitted to Geochimica et Cosmochimica Acta *June 25, 2021*
Email address: pmartinezsosa@arizona.edu (Pablo Martínez-Sosa)

Keywords: brGDGTs, lakes, Bayesian statistics, calibration

1. Introduction

Branched glycerol dialkyl glycerol tetraethers (brGDGTs) are a family of membrane-spanning lipids consisting of two alkyl chains ether-bonded to glycerol molecules on both ends. The 15 most common unique structures vary in the number (4 – 6) and position (5' or 6') of methyl groups as well as in the number of cyclopentane moieties (0 – 2) (De Jonge et al., 2013; Weijers et al., 2006). The alkyl structure and stereochemistry of the glycerol group strongly suggest a bacterial source (Weijers et al., 2006). Based on the abundance of brGDGTs in peatlands, where these molecules were first described (Sinninghe Damsté et al., 2000), Weijers et al. (2009) suggested that they were produced by Acidobacteria. Later work showed the presence of small amounts of brGDGT Ia in two bacteria from the subgroup 1 of the Acidobacteria phylum (Sinninghe Damsté et al., 2018, 2011). Nevertheless, to this day only the building blocks for brGDGTs have been found in other members of the phylum, and none of the other brGDGTs have been found in any organism.

While early literature described brGDGTs as biomarkers associated with peats and soils (Weijers et al., 2007; Sinninghe Damsté et al., 2000), later analyses have shown that these lipids can also be produced in aquatic environments such as lakes (Russell et al., 2018; Weber et al., 2015; Tierney et al., 2010; Tierney & Russell, 2009), rivers (De Jonge et al., 2014b; Zell et al., 2013), and coastal areas (Xiao et al., 2016; Zhou et al., 2014; Peterse et al., 2009). Discovery of a lacustrine-specific 5/6 methyl isomer provides further evidence of *in situ* production of brGDGTs in lakes (Weber et al., 2015), and also raises the possibility that the organisms involved in the production of these molecules in lakes might be different from those in soils.

The relative abundances of brGDGTs have been shown to change in response to both pH and temperature (Martínez-Sosa et al., 2020; Dang et al., 2018; De Jonge et al., 2014b; Tierney et al., 2010; Weijers et al., 2007). Weijers

et al. (2007) proposed the use of two indices—the cyclisation index of branched tetraethers (CBT) and methylation index of branched tetraethers (MBT)—to reflect this response. Later analytical advances using High Performance Liquid Chromatography-Mass Spectrometry (HPLC-MS) (Hopmans et al., 2016; De Jonge et al., 2014a) improved these indices by separating the 5′ and 6′ isomers. MBT'_{5Me}, a new version of MBT, was generated excluding the 6′ isomers, and CBT was replaced by CBT' which accounts for the 6′ isomers (De Jonge et al., 2014a).

Other environmental factors may also impact brGDGT distribution, such as soil moisture (Dang et al., 2016b), redox state (Weber et al., 2018), and oxygen (Martínez-Sosa & Tierney, 2019; Huguet et al., 2017; Tierney et al., 2012). Since the identity of the source organisms remains unknown (Sinninghe Damsté et al., 2018), and it has even been suggested that the production of brGDGTs could rather be an effect of microbial community changes, rather than specific organisms adapting their membranes (De Jonge et al., 2019; Weber et al., 2018), it is unclear how much impact these parameters have on the brGDGT response, or if their influence is environment-dependent, with different effects in soils and lakes.

A combination of their ubiquity, their response to changes in the environment, and their potential for preservation (Kemp et al., 2014) make brGDGTs a valuable tool for paleoclimate reconstructions. In the absence of pure culture studies, empirical calibrations are used to infer temperature and pH from brGDGT distributions. Global calibrations using the Hopmans et al. (2016) method exist for soils and peats (Dearing Crampton-Flood et al., 2020; Naafs et al., 2017a,b). However, since soil calibrations underestimate temperature when applied to lake sediments (Pearson et al., 2011; Tierney et al., 2010; Tierney & Russell, 2009; Russell et al., 2018), these cannot be used for lacustrine applications. While several local (Loomis et al., 2012; Sun et al., 2011; Tierney et al., 2010) and global (Pearson et al., 2011) lake calibrations have been presented, most of them were performed with the old analytical method and thus did not fully separate the 5' and 6' isomers. Thus far, only local calibrations

have been generated with the improved method (Russell et al., 2018; Dang et al., 2018, 2016a).

This work presents a dataset of 272 lake sediment samples, consisting of both new and previously published data, from a wide range of locations and environmental regimes. We analyze the distribution of brGDGTs in lakes and compare them to brGDGTs in soils and peats in order to better understand this proxy system. We then use our dataset to construct a new global temperature calibration. Finally, we apply our new calibration to a previously published late Holocene lake core record in order to demonstrate its applicability.

2. Methods

2.1. Samples

We analyzed 124 new, and 39 previously published (Stefanescu et al., 2021) core top (cc. top 10 cm) samples, spanning a wide range of mean annual air temperatures (MAAT), precipitation regimes and pH (Fig. 1 and Supplementary Table A.1). Samples were processed at either the University of Arizona (UA) or the University of Wyoming (UW) (Supplementary Table A.1). All samples were freeze-dried for 48 h, ground and homogenized in a solvent-cleaned mortar, and then extracted with an Accelerated Solvent Extraction (ASE) system (run at 1500 psi, 100°C, with dichloromethane:methanol (DCM: MeOH, 9:1)). At UW, the resulting total lipid extracts (TLEs) were first separated over an aminopropyl (LC-NH_2) solid phase column, using DCM:isopropanol (2:1) (neutral fraction, containing the GDGTs) then 4% acetic acid in DCM to separate the acid fraction ; this latter fraction was collected for unrelated analyses. The neutral fraction was then further separated over activated silica gel using hexane, DCM, and MeOH. At UA, the TLEs were eluted through a deactivated SiO_2 column with hexane:ethyl acetate (1:2), and dried under a N_2 stream. Both UA and UW samples were redissolved in hexane:isopropanol (99:1), and then passed through a 0.45 μm PTFE filter prior to being analyzed by HPLC. GDGTs were analyzed on an Agilent 1260 Infinity HPLC coupled to an Agilent

6120 single quadrupole mass spectrometer using two BEH HILIC silica columns (2.1×150 mm, 1.7 μm; Waters) and the methodology of Hopmans et al. (2016). We calculated peak areas using the MATLAB package ORIGAmI (Fleming & Tierney, 2016) and quantified brGDGTs by comparing the obtained peaks with a C_{46} internal standard (Huguet et al., 2006). However, our statistical analyses are based on the fractional abundances of the brGDGTs, not the absolute abundances (Supplementary Table A.2).

We supplemented our dataset with published values, including 65 samples from African lakes (Russell et al., 2018) and 49 samples from Chinese lakes (Li et al., 2017; Dang et al., 2018, 2016a). Collectively this work includes data from 272 lakes. We further compare our sediments with 663 soil and peat samples (Weijers et al., 2007; De Jonge et al., 2014a; Naafs et al., 2017b; Dearing Crampton-Flood et al., 2020) and 11 additional soil samples from Li et al. (2017).

2.2. Temperature and Precipitation Data

MAAT and mean annual precipitation (MAP) for Dang et al. (2016a), Dang et al. (2018), Li et al. (2017), and our sites were derived from either the PRISM product at 800 m resolution, for samples within the continental USA and Alaska (PRISM Climate Group, Oregon State University), or from the CRU TS 4.01 product at a resolution of 0.5° for the rest of the samples (Osborn & Jones, 2014). Values were obtained following the approach used by Dearing Crampton-Flood et al. (2020), where chordal distances were calculated for each sample. Due to the large number of samples and the wide variety of environments contained in this work, we take the parsimonious approach of using gridded air temperature as a proxy for lake surface temperature rather than constructing specific lapse rate corrections for each sample (following Dearing Crampton-Flood et al., 2020). Multiple samples within the same lake were averaged and treated as one data point, except for samples from Lake Malawi due to its large size, in which case they were kept distinct. For the Russell et al. (2018) and Dearing Crampton-Flood et al. (2020) sites we used the parameters reported by the authors. Following Dearing Crampton-Flood et al. (2020) we also calculated

the mean temperature of months above freezing (MAF). In the case of samples from Russell et al. (2018) we considered MAF to be equal to MAAT, as lakes in this region experience larger daily oscillations in temperature than seasonal, with freezing occurring only at night (Eggermont et al., 2007).

2.3. pH and Conductivity Data

Water pH was measured on site for the UW samples (Supplementary Table A.1). For the remaining samples in our dataset we collected pH and conductivity data from the literature when available (Supplementary Table A.1). We used values reported by the authors in the original work for the other datasets (Weijers et al., 2007; De Jonge et al., 2014a; Dang et al., 2016a; Li et al., 2017; Naafs et al., 2017b; Dang et al., 2018; Russell et al., 2018). We converted the reported salinity values from Li et al. (2017) to conductivity by using the Fofonoff & Millard Jr (1983) equation.

2.4. Elevation Data

Elevation for each sample was obtained from the ETOPO5 dataset (Center, 1993). Values for surface elevation were corroborated in Google Earth.

2.5. Empirical Orthogonal Function Analysis

Empirical Orthogonal Function (EOF) analysis (Lorenz, 1956), also known as Principal Component Analysis, was used to study the dataset in a reduced dimensional space. For this analysis, Singular Value Decomposition was applied to the centered covariance matrix for the fractional abundance of each brGDGT using the `svd()` *R* function. We evaluated the significance of the obtained modes by using the Rule N test (Overland & Preisendorfer, 1982). This was performed in R using 10,000 Monte Carlo simulations and a 95% confidence interval.

2.6. Indices

brGDGTs are named with roman numerals I, II, III to denote whether they contain 4, 5, or 6 methyl groups, and lowercase a, b, c to denote whether they

contain 0, 1, or 2 cyclopentane rings. In addition, the $'$ symbol is used to indicate the 6-methyl isomers (De Jonge et al., 2014a).

The MBT'_{5Me} and CBT' indices are used to quantify the relative degree of methylation and the combined cyclization and isomerization response, respectively. These were calculated following De Jonge et al. (2014a):

$$MBT'_{5Me} = \frac{(Ia + Ib + Ic)}{(Ia + Ib + Ic + IIa + IIb + IIc + IIIa)} \tag{1}$$

$$CBT' = \log_{10}\left(\frac{Ic + IIa' + IIb' + IIc' + IIIa' + IIIb' + IIIc'}{Ia + IIa + IIIa}\right) \tag{2}$$

To further investigate the role of methylation on the brGDGT species we also calculated the MBT index for the $6'$ isomers as described in Dang et al. (2016b):

$$MBT'_{6Me} = \frac{(Ia + Ib + Ic)}{(Ia + Ib + Ic + IIa' + IIb' + IIc' + IIIa')} \tag{3}$$

We also compute the isomer ratio proposed by De Jonge et al. (2014b) with the modifications made by Dang et al. (2016a), which represents the relative abundance of $6'$ isomers:

$$IR = \frac{\Sigma(II') + \Sigma(III')}{\Sigma(II) + \Sigma(III) + \Sigma(II') + \Sigma(III')} \tag{4}$$

Following Martínez-Sosa & Tierney (2019), we calculated the fractional cyclization index (fC) to quantify the relative cyclization of brGDGTs:

$$fC = \frac{\Sigma(b) + 2\Sigma(c) + \Sigma(b') + 2\Sigma(c')}{\Sigma(a) + \Sigma(b) + \Sigma(c) + \Sigma(b') + \Sigma(c')} \times 0.5 \tag{5}$$

2.7. Calibration

For the calibration of the dataset, a Bayesian model was calculated in MATLAB using the *BayMBT* package (Dearing Crampton-Flood et al., 2020) and the `baymbt_model()` function. The model is fully described in Dearing Crampton-Flood et al. (2020). Briefly, it is a simple linear regression model of the form,

$$\begin{aligned} \mathbf{y} &= \mathbf{X}\boldsymbol{\beta} + \boldsymbol{\epsilon}, \\ \boldsymbol{\epsilon} &\sim \mathcal{N}(\mathbf{0}, \sigma^2) \end{aligned} \tag{6}$$

where $\mathbf{y}$ is a $n \times 1$ vector of the MBT'_{5Me} at each n site, $\mathbf{X}$ is a $n \times 2$ matrix consisting of the corresponding environmental data (i.e., temperature or pH values) and a column of ones to represent the intercept, $\boldsymbol{\beta}$ is a 2×1 vector containing the slope and intercept terms, and $\boldsymbol{\epsilon}$ is a $n \times 1$ vector of the errors, which are assumed to be normally distributed. Priors for the slope, intercept, and error variance parameters were set to be uninformative, such that they have minimal influence on the posterior. We identified outliers from the calibration by applying the `rosnerTest` function from the *EnvStarts* R package to the residuals (Millard et al., 2018).

The Bayesian approach allows us to construct a universal lakes calibration that presents temperature as the independent variable. Since this method generates an ensemble of possible regression parameters, the calibration accounts for both parameter and residual uncertainties. Furthermore, Dearing Crampton-Flood et al. (2020) showed that the use of ordinary least squares regression with temperature as the dependent variable leads to an artifact (regression dilution) where the slope is biased toward zero because uncertainties in MBT'_{5Me} are not accounted for.

2.8. Basin Pond Core

To test our calibration, we applied it to a downcore record of MBT'_{5Me} from Basin Pond, ME, USA (Miller et al., 2018). This record spans 900 years and is one of the few lake records where the Hopmans et al. (2016) HPLC method was used. To invert our lake calibration and solve for temperature, we used the `baymbt_predict()` MATLAB function in *BayMBT*. For the prior mean value, we used the Russell et al. (2018) calibration to calculate a mean temperature for the record, and following Dearing Crampton-Flood et al. (2020) we used a prior standard deviation of 10°C. Since the standard deviation is large, this choice of prior has minimal influence on the posterior results.

We compared our reconstruction to temperature data from a nearby weather station located in Farmington, ME (Lawrimore et al., 2011), 26 km northeast of Basin Pond. The station's instrumental record spans 128 years (1891–2019)

which we used to calculate seasonal averages, MAAT and MAF.

3. Results

3.1. Environmental Parameter Distribution

MAF at our sites range from 1.6 to 28.1°C (Fig. 2a). pH values range from 4.3 to 10 (Fig. 2c), but only a few sites are truly acidic lakes (pH < 6). The available conductivity data range from 0 to 20,000,000 $\mu S/cm$ (Fig. 2d). While most of our lakes fall within the freshwater range (< 500 $\mu S/cm$), some are hypersaline or alkaline (*i.e.* Mono Lake, Lake Van, Big Soda Lake, and the Dead Sea). MAP values range from 23 to 3818 mm/year (Fig. 2e), with most of the data falling around 1000 mm/year. Our samples span a range of water depths from 0 to 377 m (Fig. 2f). The maximum depth of the lakes, where available, spans from 1 to 695 m (Fig. 2g). Finally, the elevation ranges from -462 to 4877 m.a.s.l.(Fig. 2h).

To assess the relationships between environmental parameters, we calculated the Spearman correlation for each combination of factors (Table 1). While many combinations have small and/or insignificant correlation values, we also observe some strongly correlated parameters, such as pH and conductivity (0.67), precipitation and pH (-0.48), MAF and elevation (-0.48), conductivity and elevation (-0.56), as well as precipitation and conductivity (-0.83).

3.2. BrGDGT Distribution

To assess whether brGDGT distributions are distinctively different in lakes vs. soils and peats, we compare the lake data compiled in this work with the soil and peat data from Weijers et al. (2007); De Jonge et al. (2014a); Naafs et al. (2017b); Dearing Crampton-Flood et al. (2020) and Li et al. (2017). Soils and peats show very similar distributions (not shown) so they are analyzed together.

In both datasets (Fig. 3), brGDGTs without cyclopentane rings (a compounds) have the highest fractional abundance, and the lowest abundance brGDGTs are those with two cyclopentane rings (c compounds). While brGDGT-Ia has

the highest fractional abundance in both datasets, the abundances are higher in soils and peats. A one-way t-test on this dataset also shows that soils and peats have a preference ($p < 0.05$) for $6'$ isomers. In contrast, a complementary t-test on the lake samples shows a preference for the $5'$ brGDGT isomers ($p < 0.05$).

We also observe that the lake samples have a smaller variance in the fractional abundance of each brGDGT compared with soils and peats (Fig. 3). We confirmed that this observation is statistically significant by performing a F-test ($\alpha = 0.05$) on the pooled variance of each dataset.

3.3. EOF Analysis and Correlation with Environmental Parameters

Our EOF analysis on the brGDGT fractional abundances of both the lake and soil/peat datasets, respectively, suggests that only the first two modes of each group are statistically significant based on the Rule N test. For lakes, these modes explain 58% and 24% of the variability, respectively, while for soils and peats they explain 71% and 19%. To gain better insight on the possible environmental significance of each mode, we examined the loading of each brGDGT (Fig. 4).

In the lakes dataset (Fig. 4 a and c), brGDGTs Ia and $IIIa$ load prominently on Mode 1, with opposing signs (Fig. 4a). Some other minor contributors to the mode are $IIIa'$ and IIa, with the same sign as $IIIa$; and IIa' and Ib, which load with Ia. The majority of the brGDGTs contributing to Mode 1 are used in the MBT'_{5Me} calculation (Eq. 1), with the exception of the low-abundance molecules (i.e., Ic and IIc). Mode 2 on the other hand shows that Ia, IIa and $IIIa$ load with a similar weight and sign, while Ib, IIa', IIb, IIb', and $IIIa'$ contribute with the opposite sign (Fig. 4b). The brGDGT compounds contributing to this mode are all included in the CBT' index calculation (Eq. 2).

In the soil and peat dataset (Fig. 4b and d), Mode 1 is mainly driven by brGDGT-Ia, with IIa' and $IIIa'$ plotting with the opposite sign. Mode 2 is dominated by IIa, plotting with the same sign as $IIIa$; Ia, IIa' and $IIIa'$ plot with the opposite sign.

We compared the correlations between each EOF mode and the available environmental parameters to understand the environmental processes that they might be reflecting (Table 2). Except for MAP, all variables show a significant correlation with Mode 1 of the lakes dataset, with MAF and MAAT showing the highest correlations. MAF has a stronger correlation with Mode 1 than MAAT ($\rho = 0.84$ and 0.77, respectively). Mode 2 of the lakes dataset has significant correlations with most of the environmental parameters except water depth and MAAT, but is most strongly correlated with MAP, pH and conductivity (0.58, -0.58 and -0.81, respectively). Mode 2 has a small correlation with MAF (-0.28). For soils and peats, pH has significant correlations with both Mode 1 and 2 ($\rho = 0.73$ and 0.40, respectively). MAF also shows a significant correlation with both leading modes, although relates most strongly to Mode 2 ($\rho = -0.27$ and 0.68, respectively).

3.4. Comparison with brGDGT Indices

Since the two leading modes for the lakes dataset are influenced by a set of brGDGTs similar to those that comprise the MBT'_{5Me} and CBT' indices, respectively, we compared their correlations with temperature and pH (Figs. 5 and 6). Mode 1 and MBT'_{5Me} have very similar relationships with MAAT and MAF (Fig. 5), and MAF has a higher correlation in both cases. Likewise, CBT' and Mode 2 have a comparable magnitude of correlation (0.57 and -0.58, respectively) with pH and conductivity (-0.81 and 0.83) (Fig. 6). Similar to Mode 2, CBT' has a significant correlation with all parameters but depth and MAAT (Table 3).

We also tested the correlation between other previously reported indices (MBT'_{6Me}, IR, and fC) and the environmental parameters (Table 3). IR and fC have significant correlations with all parameters except for water depth, and MBT'_{6Me} has significant correlations with all parameters except for water depth and elevation. MBT'_{6Me} shows a moderate correlation with both MAAT and conductivity (0.56 and -0.45, respectively). IR has strong correlations with MAF, pH and conductivity (0.61, 0.53, and 0.77, respectively). Finally, fC

most strongly correlates with MAF and MAAT (0.64 and 0.57, respectively). None of these indices show a better correlation with MAF or pH/conductivity than MBT'_{5Me} and CBT', respectively.

3.5. Temperature Calibration

Since MBT'_{5Me} correlates most strongly with MAF, we chose this parameter to construct our calibration. Our Bayesian model has a good fit to the data, with an $R^2 = 0.82$ and an $RMSE = 2.9$°C (Fig. 7a). The regression equation from the Bayesian model is (with 2σ uncertainties in parentheses):

$$MBT'_{5Me} = 0.030(\pm 0.001)\text{MAF} + 0.075(\pm 0.012), \quad RMSE = 0.089. \tag{7}$$

This model covers a wide range of MAF, with an upper limit of 28.1°C and a lower limit of 0°C (due to the definition of MAF). Residuals from the calibration show no significant trend (Fig. 7b). Furthermore, these residuals show no spatial pattern (not shown) nor a significant correlation with pH, precipitation, or conductivity. However, the residuals (range: -10 to 9.2°C) do have a weak but significant correlation ($p < 0.05$) with water depth ($\rho = 0.28$) and elevation ($\rho = 0.12$). As a point of comparison, we also constructed a calibration with MAAT instead of MAF (not shown). This calibration has a substantially worse performance with an $R^2 = 0.66$ and an $RMSE = 6.6$°C.

We compared the Bayesian calibrations for MBT'_{5Me} and MAF between lakes and soils/peats (Fig. 8). Soils and peats have higher average MBT'_{5Me} values than lakes for a given temperature, which leads to significantly different y-intercepts for each calibration (0.27 and 0.076 respectively). While at first glance, the slopes of regression lines for soils and lakes seem similar (0.026 and 0.030, respectively), a T-test (Long & Rippeteau, 1974) performed on the 1000-member distribution of both slope and intercept values produced by BayMBT shows that they are significantly different ($p < 0.05$). As observed by Dearing Crampton-Flood et al. (2020), the soil/peat data have a wider spread at intermediate temperatures, a feature that does not appear to be as pronounced in

the lake data (Fig. 8).

3.6. Paleoclimate Application

We applied the Bayesian calibration to the Basin Pond record (Fig. 9). Our reconstruction is similar to the one generated using the African lakes calibration Russell et al. (2018), with a mean difference in the calculated temperature of 0.9°. A reconstruction using the regression of Dang et al. (2018) plots on average 3.6°C colder than the other two reconstructions, and lies outside of the 1σ error of the Bayesian model. Dang et al. (2018) used a multiple linear regression based on fractional abundances of individual brGDGTs to generate their calibration, which explains the larger mean difference in estimated temperature to our calibration. To assess the validity of our reconstruction, we compared it with the monthly instrumental record from the weather station in Farmington, ME (26 km NE of Basin Pond). Our reconstruction plots close to the MAF calculated from the station data, and as expected, above MAAT (Fig. 9b).

3.7. Water Chemistry Calibrations

To explore whether brGDGTs in lakes can be adequately modeled by water chemistry, we computed Bayesian calibrations for CBT' using both pH and conductivity. The pH calibration (Supplementary Fig. B.1) has a weak fit and high error ($R^2 = 0.37$ and $RMSE = 1.3$). We observe a stronger fit when we use log_{10}-transformed conductivity, with an $R^2 = 0.54$ and $RMSE$ =1.04 $log_{10}(\mu S/cm)$ (Supplementary Fig. B.2). The conductivity calibration was constructed after eliminating two outlier samples: the Dead Sea and Mother Goose Lake, Alaska. The residuals for the pH calibration have a statistically significant correlation with conductivity ($\rho = -0.41$), precipitation ($\rho = 0.36$), and a weak correlation with MAF ($\rho = -0.17$). In turn, the conductivity calibration residuals show significant correlation with pH (-0.24) and MAF (-0.27).

We compared the response of CBT' to pH in lakes vs. soils and peats (Fig. 10). Soil CBT' is much more sensitive to pH than lake CBT' (slope of 0.50

vs. 0.18), leading to a much higher coefficient of determination ($R^2 = 0.73$ vs. $R^2 = 0.37$, respectively).

4. Discussion

4.1. BrGDGT Distribution

Our results show that lakes have a significantly different distribution of brGDGTs than soils and peats (Fig. 3). Overall, soils and peats have a higher fractional abundance of brGDGT-Ia, whereas lakes exhibit a higher abundance of brGDGT-$IIIa$, in line with previous studies (Buckles et al., 2014; Weber et al., 2015). Lakes also have a statistically significant preference for $5'$ isomers, in contrast to soils and peats, which are dominated by $6'$ isomers. This contrasts with the results presented by De Jonge et al. (2014b), in which river systems showed a higher abundance of $6'$ brGDGTs than soils, but agrees with De Jonge et al. (2014a), where soils show similar abundances of $6'$ isomers to $5'$. brGDGTs in the lake sediments have statistically significant lower dispersion (variance) than those in the soils and peats (Fig. 3).

These differences in both brGDGT distribution and dispersion support the hypothesis that in situ production dominates brGDGT distribution in lake sediments on the global scale (Tierney & Russell, 2009; Buckles et al., 2014; Weber et al., 2015). Were soil input dominant, we would expect to see equivalent amounts of $5'$ and $6'$ isomers in lakes, and higher, not lower variance in brGDGT distributions. This does not exclude the possibility that soil GDGT input might still be important for certain lacustrine environments (e.g., Li et al., 2017), but supports the general applicability of a global, lakes-specific calibration.

4.2. EOF Modes

Our EOF analysis shows that a substantial amount of the variability in our lake (83%) and the soil–peat dataset (90%) can be explained by the first two modes. Since the obtained modes are orthogonal by definition, they represent independent drivers for the data. We observe that temperature and water chemistry (pH and conductivity), respectively, have a high correlation with these

main two modes, suggesting that much of the variance in the brGDGT datasets can be explained by these factors, at least on a global scale. While co-correlated environmental drivers could also play a role, for our lacustrine samples none of the other environmental parameters investigated here have a particularly high correlation with MAF and pH/conductivity, respectively, with the exception of precipitation (Table 1). However, the strong correlation between precipitation and conductivity simply reflects the fact that more saline lakes are found in arid places. It is much more likely that water chemistry exerts the direct control on brGDGT producers living in lakes than precipitation.

4.2.1. Mode 1

Of the two modes, Mode 1 explains most of the variance (58% and 71% in lakes and soils, respectively) suggesting that the phenomena captured by this mode dominate the brGDGT response.

In lakes, we interpret Mode 1 to reflect the influence of temperature on brGDGT distributions. It strongly correlates with both MAAT and MAF, and has smaller correlations with pH and conductivity (Table 2). In addition, the brGDGTs that load most prominently on Mode 1 (Fig. 4a) are similar to those involved in the calculation of MBT'_{5Me} (Equation 1), the established index for relative methylation that has already been shown to respond to temperature. Morever, laboratory incubations provide direct evidence that temperature influences brGDGT methylation (Martínez-Sosa et al., 2020).

While Mode 1 and MBT'_{5Me} share the major contributors (Ia, Ib, IIa, $IIIa$), the remaining brGDGT compounds behave slightly differently; IIb and IIc contribute to MBT'_{5Me}, while $IIIa'$ and IIa' contribute to Mode 1. The fact that these latter compounds load on Mode 1 suggests that, contrary to the assumption that the temperature sensitivity is limited to the 5-methyl brGDGTs, 6-methyl brGDGTs may also be slightly temperature sensitive, at least in lakes (Dang et al., 2018). Controlled incubations of lake water also show that $6'$ isomers increase in concentration with temperature (Martínez-Sosa et al., 2020), supporting this interpretation. Nevertheless, the EOF analysis suggests that the

6′ isomers are still minor contributors to the temperature response. Furthermore, Mode 1 and MBT'_{5Me} have near identical correlations with temperatures (Fig. 5), which suggests to us that the inclusion of additional brGDGTs in Mode 1 does not provide substantial additional information. Given the widespread use of MBT'_{5Me} (and the fact that our Mode 1 is nearly identical) we consider it the preferred metric for capturing the temperature sensitivity of brGDGT distributions and use it for further analyses in this work.

Both Mode 1 and MBT'_{5Me} have a stronger correlation with MAF than MAAT (Fig. 5). In particular, the use of MAF brings the colder lakes from the East African dataset (Russell et al., 2018) (which do not freeze on a seasonal basis) into alignment with the seasonally-frozen mid- and high-latitude lakes in the rest of the dataset. This could suggests that brGDGT producers are limited to a growing season; i.e., may not be active when lakes are frozen during the winter (Miller et al., 2018; Loomis et al., 2014), or that brGDGTs are unable to record temperatures below freezing due to the ice cover decoupling air-water temperatures (Cao et al., 2020). While previous studies have suggested that no seasonality is observed in soils (Weijers et al., 2011; Lei et al., 2016), these results contrast with others where a better agreement between the warm season is observed in soils and peats, suggesting that that the producers are less active at below-freezing temperatures (Dearing Crampton-Flood et al., 2020; Naafs et al., 2017a).

In contrast with lakes, Mode 1 for soils and peats is more closely related to pH and only weakly correlated with temperature. The pattern of the brGDGT loadings on this Mode (Fig. 4b) resembles the CBT' equation (Equation 2), further suggesting that pH is the dominant influence on soil and peat brGDGT distributions. This is in agreement with De Jonge et al. (2014a), who also found that the leading principal component of brGDGTs in soils was associated with pH, and previous synthesis work that emphasizes the strong influence of pH on peat (Naafs et al., 2017b) and soil brGDGT distributions (Naafs et al., 2017a; Xiao et al., 2015). This represents a fundamental difference from brGDGTs in lake sediments, which, as our EOF analysis highlights, are more sensitive to

459 temperature.

460 *4.2.2. Mode 2*

461 For lakes, we interpret Mode 2 as a reflection of water chemistry, as it is
462 strongly correlated with lake pH and conductivity (Fig. 6 and Table 2). While
463 no correlation with MAAT is observed, Mode 2 does have a significant, but
464 weak, correlation with MAF ($\rho = -0.28$), however this most likely reflects
465 the correlation between MAF and both pH and conductivity present in our
466 environmental data (Table 1). CBT', which has been used as a pH index,
467 behaves similarly to Mode 2 (Table 3), and the two indices are influenced by
468 the same group of brGDGTs (Fig. 4b and Equation 2), with a few exceptions
469 (Ib and IIb participate in Mode 2). The correlations with conductivity (ca.
470 0.8) are much higher than with pH (0.58) for both Mode 2 and CBT', which
471 could suggest that brGDGT distributions are sensitive other ionic constituents
472 in addition to the acidity of the water. However, since pH and conductivity are
473 closely linked, it is difficult to discern a causal relationship from the strength of
474 these correlations with the data presented here. The strong relationship with
475 conductivity could simply reflect the fact that this measurement is easier to make
476 in the field than pH, and potentially more accurate (since pH meters need to be
477 calibrated). Furthermore, we have fewer measurements of conductivity (N=130)
478 than pH (N=189), which could inflate the correlation value for conductivity.

479 Mode 2 explains a much smaller percentage of the variance (24%) than Mode
480 1, indicating that pH and/or water chemistry does not have a strong influence
481 on brGDGTs. This might explain the ambiguous pH response observed in other
482 empirical lake studies (Russell et al., 2018; Sun et al., 2011), as well as in
483 controlled incubations of lake water (Martínez-Sosa et al., 2020). Given that our
484 dataset spans a large pH range (4.3–10) it is unlikely that the weak relationship
485 we observe is due to sampling bias. It is possible that the strong correlation with
486 pH in soils and peats partly reflects an effect of soil moisture (Naafs et al., 2017a;
487 Dang et al., 2016a), which is lost in lacustrine environments. Another possibility,
488 supported by previous works (De Jonge et al., 2019; Weber et al., 2018), is that

the microbial communities responsible for producing brGDGTs in soils and lakes are different, and thus have characteristic responses to temperature and pH.

Mode 2 in the soils and peats dataset is related to temperature, with a pattern of loadings that closely resembles the equation for MBT'_{5Me} (Fig. 4d). This mode only explains 19% of the variance in the data, which agrees with the fact that temperature predictability from soil and peat brGDGTs remains limited (i.e., RMSE is ca. 4°C) by the large amount of scatter in the MBT'_{5Me}-temperature relationship (Dearing Crampton-Flood et al., 2020). Ultimately, soils and peats are more strongly influenced by pH than temperature, whereas the inverse is true for lakes.

4.3. Additional Indices

IR and fC, indices for the relative degree of isomerization and cyclization, show moderately strong correlations with MAF, conductivity, and pH (Table 3). The observed relationship to temperature supports our previous microcosm results, which similarly indicate that isomerization and cyclization have thermal sensitivity (Martínez-Sosa et al., 2020). However, since water chemistry exerts an equal (if not larger, in the case of IR) influence on these indices, they are not as useful as MBT'_{5Me} for paleothermometry. Conversely, the influence of temperature limits the utility of IR and fC for water chemistry reconstruction (pH or conductivity), even when IR show values close to those from CBT'. As discussed, the sensitivity of brGDGTs to water chemistry is better captured by CBT', which is a combined metric of isomerization and cyclization.

4.4. Temperature Calibration

Our EOF analysis demonstrates that temperature is the primary influence on brGDGT distribution in lakes on the global scale, and further suggests that the use of MAF, rather than MAAT, is most appropriate for a global calibration. This is probably because MAF accounts for the seasonally-biased response observed in the mid to high latitudes, which likely reflects reduced microbial activity during winter (Dearing Crampton-Flood et al., 2020).

Our MAF calibration (Fig. 7) has an $R^2 = 0.82$, comparable with previous calibrations (Dearing Crampton-Flood et al., 2020; Naafs et al., 2017a; De Jonge et al., 2014a) but lower than the one presented by Russell et al. (2018) of 0.92. This likely reflects the larger number of samples in this work, which also span a greater diversity of climate and geography. Despite this, both calibrations have comparable RMSE values (2.4°C and 2.9°C). In contrast, if we construct a calibration with MAAT, we get a substantially worse fit, with an $R^2 = 0.66$ and a large RMSE (6.6°C). As noted above in the discussion of the EOF results, this is because cold, tropical lakes and cold, mid-latitude lakes are offset from each other when using MAAT (see also Fig. 5). This further supports calibration to MAF.

In the process of developing the temperature calibration, a Rosner test (Rosner, 1983) identified five outliers (Fig. 7a), which we ultimately excluded from the final calibration. These outliers do not come from the same study, which suggests they are not related to laboratory-specific procedures. Rather, they seem to be related to extreme water chemistry—four out of five of the outliers come from alkaline, saline lakes. Two of the outlying samples are from the western USA: Mono Lake and Big Soda Lake. Mono lake has a pH of 9.7 and conductivity of 80,000 $\mu S/cm$ (Jiang et al., 2004; Domagalski et al., 1989), and Big Soda lake has a pH of 9.7 and conductivity of about 20,000 $\mu S/cm$ (Priscu et al., 1982; Kharaka et al., 1984). Big Soda Lake also has an unusual dichothermal water column profile as a consequence of its high salt content (Priscu et al., 1982), which might influence both the microbial communities present and the brGDGTs response. Two additional outliers come from Chile: Laguna Amarga and Laguna del Negro Francisco. Both are shallow (4.1 and 1 m, maximum depth respectively) endorheic basins. Laguna Amarga has a pH of 8.4 and a conductivity of 52,367 $\mu S/cm$) (Campos et al., 1995), while Laguna del Negro Francisco is a hypersaline (80,000 $\mu S/cm$) lagoon (Grosjean et al., 1997). The fifth outlier, Mahuhura lake from Uganda, is the only outlying site that is not saline; its conductivity is 600 $\mu S/cm$. However, it is alkaline, with a pH of 8.9 (Gelorini et al., 2011).

While the observed outliers are nearly all highly alkaline/saline lakes, it is important to note that there are other lakes in our dataset that have either high pH (i.e. Lake Van with pH = 9.8) or high conductivity (i.e. Lake Daihai, 15,647 $\mu S/cm$) and fall well within the confidence interval of our calibration. Our calibration also includes a sample from the Dead Sea (Neugebauer et al., 2014), which has an extremely high conductivity of 202 mS/cm (Akawwi et al., 2011) but a pH of only 6 (Sass & Ben-Yaakov, 1977). This sample, while on the margin of our confidence interval, is not an outlier, which suggests that it is the combined effect of salinity and alkalinity that leads to outlying brGDGT distributions. Our observation that alkaline, saline lakes tend to have outlying correlations between brGDGT and temperature is in line with results presented by Tierney et al. (2010), in which lakes from Africa with conductivities above 30,000 $\mu S/cm$ showed distinct brGDGT distributions compared with the rest of the dataset (<5,900 $\mu S/cm$).

There are several possible explanations for the deviant behavior of brGDGT distributions in alkaline, saline lakes. For one, these types of lakes have a restricted bacterial diversity (Humayoun et al., 2003), so the microbial community responsible for the brGDGT production in these environments might be distinct from the communities found in more neutral, freshwater lakes, and thus may have a completely different sensitivity to environmental perturbations. Alternatively, allochthonous soil brGDGTs might dominate distributions in saline, alkaline lakes because the environment is not favorable for the brGDGT producing organisms. Indeed, except for Mahuhura, the MBT'_{5Me} values in our outlying lakes are situated in the upper left-hand quadrant of the regression, closer to the soil calibration line (Fig. 7), and, like soils, the outlying lakes show a higher relative abundance of brGDGT-Ia and a preference for the 6′ methyl isomers (Fig. 11). This interpretation is supported by Li et al. (2017), who noted that the soil brGDGT regression was applicable to their data from alkaline lakes. However, the samples from Li et al. (2017) seem to fall within the confidence interval of our regression, despite most lakes having a pH above 9.3 and conductivity values between 1,590 and 275,950 $\mu S/cm$. This suggests a

more complicated interaction between brGDGT distributions and water chemistry (i.e., the concentrations of specific ions) that deserves further attention in future work.

Alkaline, saline environments aside, the good fit of our model to globally-distributed values of MBT'_{5Me} demonstrates that brGDGT response to temperature is mostly unaffected by additional physical and chemical factors. Further evidence of this comes from the weak and statistically insignificant correlations between the model residuals and most environmental parameters ($\rho < 0.05$, not shown). There is a weak correlation between our model residuals and water depth ($\rho = 0.28$). Notably, the correlation with water depth is significant only for shallow (< 20 m) lakes ($\rho = 0.27$, Fig. 12a), not deep lakes ($\rho = -0.14$, Fig. 12a). The correlation is such that the shallowest lakes have negative residuals, indicating that brGDGTs predict higher-than-expected temperatures. Investigating this relationship further, we found that the correlation is stronger ($\rho = 0.40$) if we consider only the temperate lakes ($> 35°$N and S) within our data set ($n = 108$; Fig. 12b), and is not significant for the shallow tropical lakes ($n = 82$). We attribute this to an increased influence of thermal variability in temperate lakes. Unlike tropical lakes, which experience restricted seasonal changes in air temperature (Russell et al., 2018), temperate lakes—especially shallow ones, which lack the volume to buffer this thermal effect—are subject to large swings in temperature both seasonally and diurnally. Thus the apparent influence of water depth on brGDGT distributions in shallow temperate lakes could reflect water temperatures that seasonally or diurnally exceed MAF. Alternatively, the observed warm bias could indicate greater input of soil-derived brGDGTs in shallow lake systems. However, were this the case, we would expect to see a similar phenomenon in shallow tropical lakes, where there is a clear offset between soil and lake brGDGTs (Tierney et al., 2010; Russell et al., 2018). A third possibility is that the trend from negative to positive residuals reflects an increasing contribution of *in situ* production at depth (i.e., at or near the thermocline), which would result in lower inferred temperatures in deeper lakes. However, if this were the primary explanation, we would expect to see

the residual trend persist in deeper lakes, where the thermocline temperatures can be much lower than surface temperatures. Although it is a relatively minor effect, this observed influence of water depth on lacustrine brGDGTs has also been observed in other work (Stefanescu et al., 2021) and deserves further investigation.

If we compare the lake and soil/peat MBT'_{5Me} calibrations, we find that soils and peats have a reduced sensitivity (i.e., lower slope) to temperature (Figure 8). There is also a large difference in the y-intercept terms between the models, which reflects the tendency of lacustrine environments to have lower MBT'_{5Me} values compared with soils at a given temperature – the so-called "cold bias" (Russell et al., 2018; Tierney et al., 2010). The lakes regression also has a lower error (RMSE = 2.9°C) than the soils model (RMSE = 3.9°C). These distinctive characteristics support the hypothesis that the microbial communities responsible for the production of brGDGTs in soils and lakes might be different (De Jonge et al., 2019; Weber et al., 2018, 2015), and/or that other interfering factors, such as soil moisture (Dang et al., 2016b) affect the sensitivity of brGDGTs in soils.

Incubations of lake water at controlled temperatures (Martínez-Sosa et al., 2020) (Fig. 8, purple squares), generally plot close to the lake sediment dataset, which suggests that the regression line adequately captures the in situ response of lake brGDGTs. The incubation datapoint at 9°C is an exception—it plots closer to the soils. However, no substantial increase in brGDGT concentration was detected in the 9°C incubation (Martínez-Sosa et al., 2020), thus we suspect that the brGDGT producers were not active at this temperature.

4.5. Paleoclimate Application

When we apply our new temperature calibration to brGDGTs at Basin Pond, we obtain temperatures that are on average ~ 0.9°C lower than the Russell et al. (2018) calibration (Fig. 9a). However, since our calibration includes a larger variety of geographic and environmental settings, including samples from the northeast USA, it might be more appropriate for the Basin Pond site. Even

though the lake core has a lower resolution than the instrumental record, MAF values from the latter fall within the 1σ range of our reconstruction, with an average difference of 1°C. This suggests that our new global calibration provides reasonably accurate estimates of MAF.

4.6. Water Chemistry Calibrations

Our EOF analysis demonstrates that water chemistry (Mode 2) impacts brGDGT distributions, but not nearly as strongly as temperature. Accordingly, calibrations for both pH and conductivity have low coefficients of determination ($R^2 = 0.37$ and 0.54, respectively (Supplementary B.1 and B.1). The pH calibration in particular has an RMSE of 1.3 pH units, suggesting that it is not very precise.

In contrast to the MAF calibration, both the pH and conductivity calibrations residuals have statistically significant correlations with several other environmental parameters (MAF, precipitation, and each other). We hypothesize that this is due to the partial correlation between pH and conductivity ($\rho = 0.67$), and the relatively low percentage of explained variance that these parameters appear to be responsible for (24%) (if they are equated with Mode 2).

Given the weak fit, large errors, and correlation with other environmental parameters, we do not recommend the use of the water chemistry calibrations for paleoclimate reconstruction. An exception might be cases where changes in pH and conductivity in the paleoenvironment are expected to be large (i.e., thus swamping out the high RMSE).

Soils and peats have a much stronger relationship with pH than lakes ($\rho =$ 0.82 vs 0.53), with a dramatically different regression line (Fig. 10). This, once again, could be explained by different organisms in soils and lakes, and/or the impact of soil moisture (which does not affect lake brGDGTs), and further supports the idea that soil input has only a small influence on lacustrine brGDGTs globally.

5. Conclusions

In this work we present a globally distributed dataset of brGDGTs in lacustrine core top sediments. In agreement with previous empirical and laboratory studies we find that temperature, particularly the mean temperature above freezing, has the largest influence on the brGDGT response. Our EOF analysis corroborates that the molecules involved in the MBT'_{5Me} calculation show the best correlation with temperature. Water chemistry, either pH or conductivity, exerts a weaker influence on brGDGT distributions. While pH and conductivity calibrations are presented in this work, they have relatively poor predictability, so they should be used with caution until further work has been done to investigate the influence of water chemistry on brGDGTs from a first principles perspective.

Comparison of our lake dataset with soils and peats suggests that the brGDGT response in lakes is consistently different—in distribution, variance, and correlation to environmental factors. This supports the hypothesis that brGDGTs in lakes are, in most cases, produced in situ, possibly by a distinct microbial community. However, this does exclude the possibility that in some particular lake environments soil inputs might dominate. We hypothesize that this may be the case for alkaline/saline lakes, given that they tend to be outliers, and their brGDGTs distributions are more similar to those of soils.

Finally, our global Bayesian calibration improves on previous works by expanding the sample size and number of locations, accounting for uncertainties in both the calibration parameters and residual error, as well as resolving the regression dilution bias that emerges in traditional ordinary least squares models. While care should be taken when working with highly alkaline, hypersaline systems, the Bayesian lake calibration presented here is robust across a wide range of environmental regimes. The lakes BayMBT model has a steeper slope and lower intercept than the soil model, which suggests that soil- or lake-specific calibrations should be applied only to appropriate sample sets whenever possible to obtain the most accurate temperature estimation.

6. Research Data

Data associated with article is available on GitHub, and on the Pangaea database.

Acknowledgments

We thank the LacCore facility for providing the samples used in this work. We also acknowledge Patrick Murphy for his assistance with the lipid analysis, and Darrell Kaufman for making the Alaskan surface sediments available. This research was funded by the National Science Foundation, grant EAR-1603674 and grant EPS-1655726, and by CONACYT through the student scholarship 440897.

References

Akawwi, E., Al-Zoubi, A., & Abueladas, A.-R. (2011). Using electrical conductivity for locating the submarine groundwater discharge along the eastern shores of the Dead Sea-Jordan. *Int. Multidiscip. Sci. Geoconf. SGEM*, *1*, 653.

Buckles, L. K., Weijers, J. W., Verschuren, D., & Sinninghe Damsté, J. S. (2014). Sources of core and intact branched tetraether membrane lipids in the lacustrine environment: Anatomy of lake challa and its catchment, equatorial east africa. *Geochimica et Cosmochimica Acta*, *140*, 106–126.

Campos, H., Soto, D., Parra, O., Steffen, W., & Aguero, G. (1995). Limnological studies of Amarga lagoon, Chile: a saline lake in Patagonian South America. *Int. J. Salt Lake Res.*, *4*, 301–314.

Cao, J., Rao, Z., Shi, F., & Jia, G. (2020). Ice formation on lake surfaces in winter causes warm-season bias of lacustrine brGDGT temperature estimates. *Biogeosciences*, *17*.

Center, N. G. D. (1993). 5-minute gridded global relief data (etopo5).

Dang, X., Ding, W., Yang, H., Pancost, R. D., Naafs, B. D. A., Xue, J., Lin, X., Lu, J., & Xie, S. (2018). Different temperature dependence of the bacterial brGDGT isomers in 35 Chinese lake sediments compared to that in soils. *Org. Geochem.*, *119*, 72–79.

Dang, X., Xue, J., Yang, H., & Xie, S. (2016a). Environmental impacts on the distribution of microbial tetraether lipids in Chinese lakes with contrasting pH: Implications for lacustrine paleoenvironmental reconstructions. *Sci. China Earth Sci.*, *59*, 939–950.

Dang, X., Yang, H., Naafs, B. D. A., Pancost, R. D., & Xie, S. (2016b). Evidence of moisture control on the methylation of branched glycerol dialkyl glycerol tetraethers in semi-arid and arid soils. *Geochim. Cosmochim. Acta*, *189*, 24–36.

De Jonge, C., Hopmans, E. C., Stadnitskaia, A., Rijpstra, W. I. C., Hofland, R., Tegelaar, E., & Sinninghe Damsté, J. S. (2013). Identification of novel penta-and hexamethylated branched glycerol dialkyl glycerol tetraethers in peat using HPLC–MS2, GC–MS and GC–SMB-MS. *Org. Geochem.*, *54*, 78–82.

De Jonge, C., Hopmans, E. C., Zell, C. I., Kim, J.-H., Schouten, S., & Sinninghe Damsté, J. S. (2014a). Occurrence and abundance of 6-methyl branched glycerol dialkyl glycerol tetraethers in soils: Implications for palaeoclimate reconstruction. *Geochim. Cosmochim. Acta*, *141*, 97–112.

De Jonge, C., Radujković, D., Sigurdsson, B. D., Weedon, J. T., Janssens, I., & Peterse, F. (2019). Lipid biomarker temperature proxy responds to abrupt shift in the bacterial community composition in geothermally heated soils. *Org. Geochem.*, .

De Jonge, C., Stadnitskaia, A., Hopmans, E. C., Cherkashov, G., Fedotov, A., & Sinninghe Damsté, J. S. (2014b). In situ produced branched glycerol dialkyl glycerol tetraethers in suspended particulate matter from the Yenisei River, Eastern Siberia. *Geochim. Cosmochim. Acta*, *125*, 476–491.

754 Dearing Crampton-Flood, E., Tierney, J. E., Peterse, F., Kirkels, F. M., &
755 Damsté, J. S. S. (2020). Baymbt: A bayesian calibration model for branched
756 glycerol dialkyl glycerol tetraethers in soils and peats. *Geochim. Cosmochim.*
757 *Acta*, *268*, 142–159.

758 Domagalski, J. L., Orem, W. H., & Eugster, H. P. (1989). Organic geochemistry
759 and brine composition in Great Salt, Mono, and Walker Lakes. *Geochim.*
760 *Cosmochim. Acta*, *53*, 2857–2872.

761 Eggermont, H., Russell, J. M., Schettler, G., Van Damme, K., Bessems, I., &
762 Verschuren, D. (2007). Physical and chemical limnology of alpine lakes and
763 pools in the Rwenzori Mountains (Uganda–DR Congo). *Hydrobiologia*, *592*,
764 151–173.

765 Fleming, L. E., & Tierney, J. E. (2016). An automated method for the deter-
766 mination of the TEX_{86} and paleotemperature indices. *Org. Geochem.*, *92*,
767 84–91.

768 Fofonoff, N. P., & Millard Jr, R. (1983). Algorithms for the computation of
769 fundamental properties of seawater.

770 Gelorini, V., Verbeken, A., van Geel, B., Cocquyt, C., & Verschuren, D. (2011).
771 Modern non-pollen palynomorphs from East African lake sediments. *Rev.*
772 *Palaeobot. Palynol.*, *164*, 143–173.

773 Grosjean, M., Valero-Garcés, B. L., Geyh, M. A., Messerli, B., Schotterer, U.,
774 Schreier, H., & Kelts, K. (1997). Mid-and late-Holocene limnogeology of La-
775 guna del Negro Francisco, northern Chile, and its palaeoclimatic implications.
776 *The Holocene*, *7*, 151–159.

777 Hopmans, E. C., Schouten, S., & Sinninghe Damsté, J. S. (2016). The effect
778 of improved chromatography on GDGT-based palaeoproxies. *Org. Geochem.*,
779 *93*, 1–6.

780 Huguet, A., Meador, T. B., Laggoun-Défarge, F., Könneke, M., Wu, W.,
781 Derenne, S., & Hinrichs, K.-U. (2017). Production rates of bacterial tetraether

lipids and fatty acids in peatland under varying oxygen concentrations. *Geochim. Cosmochim. Acta*, *203*, 103–116.

Huguet, C., Hopmans, E. C., Febo-Ayala, W., Thompson, D. H., Sinninghe Damsté, J. S., & Schouten, S. (2006). An improved method to determine the absolute abundance of glycerol dibiphytanyl glycerol tetraether lipids. *Org. Geochem.*, *37*, 1036–1041.

Humayoun, S. B., Bano, N., & Hollibaugh, J. T. (2003). Depth distribution of microbial diversity in Mono Lake, a meromictic soda lake in California. *Appl. Environ. Microbiol.*, *69*, 1030–1042.

Jiang, S., Steward, G., Jellison, R., Chu, W., & Choi, S. (2004). Abundance, distribution, and diversity of viruses in alkaline, hypersaline Mono Lake, California. *Microb. Ecol.*, *47*, 9–17.

Kemp, D. B., Robinson, S. A., Crame, J. A., Francis, J. E., Ineson, J., Whittle, R. J., Bowman, V., & O'Brien, C. (2014). A cool temperate climate on the Antarctic Peninsula through the latest Cretaceous to early Paleogene. *Geology*, *42*, 583–586.

Kharaka, Y. K., Robinson, S. W., Law, L. M., & Carothers, W. W. (1984). Hydrogeochemistry of Big Soda Lake, Nevada: an alkaline meromictic desert lake. *Geochim. Cosmochim. Acta*, *48*, 823–835.

Lawrimore, J. H., Menne, M. J., Gleason, B. E., Williams, C. N., Wuertz, D. B., Vose, R. S., & Rennie, J. (2011). An overview of the Global Historical Climatology Network monthly mean temperature data set, version 3. *J. Geophys. Res.*, *116*.

Lei, Y., Yang, H., Dang, X., Zhao, S., & Xie, S. (2016). Absence of a significant bias towards summer temperature in branched tetraether-based paleothermometer at two soil sites with contrasting temperature seasonality. *Organic Geochemistry*, *94*, 83–94.

Li, J., Naafs, B. D. A., Pancost, R. D., Yang, H., Liu, D., & Xie, S. (2017). Distribution of branched tetraether lipids in ponds from Inner Mongolia, NE China: Insight into the source of brGDGTs. *Org. Geochem.*, *112*, 127–136.

Long, A., & Rippeteau, B. (1974). Testing contemporaneity and averaging radiocarbon dates. *Am. Antiq.*, *39*, 205–215.

Loomis, S. E., Russell, J. M., Heureux, A. M., D'Andrea, W. J., & Damsté, J. S. S. (2014). Seasonal variability of branched glycerol dialkyl glycerol tetraethers (brGDGTs) in a temperate lake system. *Geochim. Cosmochim. Acta*, *144*, 173–187.

Loomis, S. E., Russell, J. M., Ladd, B., Street-Perrott, F. A., & Damsté, J. S. S. (2012). Calibration and application of the branched GDGT temperature proxy on East African lake sediments. *Earth Planet. Sci. Lett.*, *357*, 277–288.

Lorenz, E. N. (1956). Empirical orthogonal functions and statistical weather prediction. Statistical Forecasting Project Rep. 1,MIT Department of Meteorology.

Martínez-Sosa, P., & Tierney, J. E. (2019). Lacustrine brGDGT response to microcosm and mesocosm incubations. *Org. Geochem.*, *127*, 12–22.

Martínez-Sosa, P., Tierney, J. E., & Meredith, L. K. (2020). Controlled lacustrine microcosms show a brGDGT response to environmental perturbations. *Org. Geochem.*, (p. 104041).

Millard, S. P., Kowarik, M. A., & Imports, M. (2018). Package 'EnvStats'.

Miller, D. R., Habicht, M. H., Keisling, B. A., Castañeda, I. S., & Bradley, R. S. (2018). A 900-year New England temperature reconstruction from in situ seasonally produced branched glycerol dialkyl glycerol tetraethers (brGDGTs). *Clim. Past*, *14*, 1653–1667.

Naafs, B., Gallego-Sala, A., Inglis, G., & Pancost, R. (2017a). Refining the global branched glycerol dialkyl glycerol tetraether (brGDGT) soil temperature calibration. *Org. Geochem.*, *106*, 48–56.

837 Naafs, B., Inglis, G., Zheng, Y., Amesbury, M., Biester, H., Bindler, R., Blewett,
838 J., Burrows, M., del Castillo Torres, D., Chambers, F., Cohen, A., Ever-
839 shed, R., Feakins, S., Gałka, M., Gallego-Sala, A., Gandois, L., Gray, D.,
840 Hatcher, P., Coronado, E. H., Hughes, P., Huguet, A., Könönen, M., Laggoun-
841 Défarge, F., Lähteenoja, O., Lamentowicz, M., Marchant, R., McClymont, E.,
842 Pontevedra-Pombal, X., Ponton, C., Pourmand, A., Rizzuti, A., Rochefort,
843 L., Schellekens, J., Vleeschouwer, F. D., & Pancost, R. (2017b). Introduc-
844 ing global peat-specific temperature and pH calibrations based on brGDGT
845 bacterial lipids. *Geochim. Cosmochim. Acta*, *208*, 285–301.

846 Neugebauer, I., Brauer, A., Schwab, M. J., Waldmann, N. D., Enzel, Y., Kita-
847 gawa, H., Torfstein, A., Frank, U., Dulski, P., Agnon, A. et al. (2014). Lithol-
848 ogy of the long sediment record recovered by the ICDP Dead Sea Deep Drilling
849 Project (DSDDP). *Quat. Sci. Rev.*, *102*, 149–165.

850 Osborn, T., & Jones, P. (2014). The CRUTEM4 land-surface air temperature
851 data set: construction, previous versions and dissemination via Google Earth.
852 *Earth Syst. Sci. Data*, *6*, 61–68.

853 Overland, J. E., & Preisendorfer, R. (1982). A significance test for principal
854 components applied to a cyclone climatology. *Mon. Weather Rev.*, *110*, 1–4.

855 Pearson, E. J., Juggins, S., Talbot, H. M., Weckström, J., Rosén, P., Ryves,
856 D. B., Roberts, S. J., & Schmidt, R. (2011). A lacustrine GDGT-temperature
857 calibration from the Scandinavian Arctic to Antarctic: Renewed potential for
858 the application of GDGT-paleothermometry in lakes. *Geochim. Cosmochim.*
859 *Acta*, *75*, 6225–6238.

860 Peterse, F., Kim, J.-H., Schouten, S., Kristensen, D. K., Koç, N., & Damsté,
861 J. S. S. (2009). Constraints on the application of the MBT/CBT palaeother-
862 mometer at high latitude environments (Svalbard, Norway). *Org. Geochem.*,
863 *40*, 692–699.

864 Priscu, J., Axler, R., Carlton, R., Reuter, J., Arneson, P., & Goldman,

C. (1982). Vertical profiles of primary productivity, biomass and physico-chemical properties in meromictic Big Soda Lake, Nevada, USA. *Hydrobiologia*, *96*, 113–120.

PRISM Climate Group, Oregon State University (). http://prism.oregonstate.edu. Created 4 Dec 2018.

Rosner, B. (1983). Percentage points for a generalized ESD many-outlier procedure. *Technometrics*, *25*, 165–172.

Russell, J. M., Hopmans, E. C., Loomis, S. E., Liang, J., & Damsté, J. S. S. (2018). Distributions of 5- and 6-methyl branched glycerol dialkyl glycerol tetraethers (brGDGTs) in East African lake sediment: Effects of temperature, pH, and new lacustrine paleotemperature calibrations. *Org. Geochem.*, *117*, 56–69.

Sass, E., & Ben-Yaakov, S. (1977). The carbonate system in hypersaline solutions: Dead Sea brines. *Mar. Chem.*, *5*, 183–199.

Sinninghe Damsté, J. S., Hopmans, E. C., Pancost, R. D., Schouten, S., & Geenevasen, J. A. (2000). Newly discovered non-isoprenoid glycerol dialkyl glycerol tetraether lipids in sediments. *Chem. Commun.*, (pp. 1683–1684).

Sinninghe Damsté, J. S., Rijpstra, W. I. C., Foesel, B. U., Huber, K. J., Overmann, J., Nakagawa, S., Kim, J. J., Dunfield, P. F., Dedysh, S. N., & Villanueva, L. (2018). An overview of the occurrence of ether-and ester-linked iso-diabolic acid membrane lipids in microbial cultures of the Acidobacteria: Implications for brGDGT paleoproxies for temperature and pH. *Org. Geochem.*, *124*, 63–76.

Sinninghe Damsté, J. S., Rijpstra, W. I. C., Hopmans, E. C., Weijers, J. W., Foesel, B. U., Overmann, J., & Dedysh, S. N. (2011). 13, 16-Dimethyl octacosanedioic acid (iso-diabolic acid), a common membrane-spanning lipid of Acidobacteria subdivisions 1 and 3. *Appl. Environ. Microbiol.*, *77*, 4147–4154.

892 Stefanescu, I. C., Shuman, B. N., & Tierney, J. E. (2021). Temperature and wa-
893 ter depth effect on brGDGT distributions in sub-alpine lakes of mid-latitude
894 North America. *Organic Geochemistry*, *152*, 104174.

895 Sun, Q., Chu, G., Liu, M., Xie, M., Li, S., Ling, Y., Wang, X., Shi, L., Jia,
896 G., & Lue, H. (2011). Distributions and temperature dependence of branched
897 glycerol dialkyl glycerol tetraethers in recent lacustrine sediments from China
898 and Nepal. *JGR*, *116*.

899 Tierney, J. E., & Russell, J. M. (2009). Distributions of branched GDGTs in a
900 tropical lake system: implications for lacustrine application of the MBT/CBT
901 paleoproxy. *Org. Geochem.*, *40*, 1032–1036.

902 Tierney, J. E., Russell, J. M., Eggermont, H., Hopmans, E., Verschuren,
903 D., & Sinninghe Damsté, J. S. (2010). Environmental controls on
904 branched tetraether lipid distributions in tropical East African lake sediments.
905 *Geochim. Cosmochim. Acta*, *74*, 4902–4918.

906 Tierney, J. E., Schouten, S., Pitcher, A., Hopmans, E. C., & Sinninghe Damsté,
907 J. S. (2012). Core and intact polar glycerol dialkyl glycerol tetraethers
908 (GDGTs) in Sand Pond, Warwick, Rhode Island (USA): Insights into the
909 origin of lacustrine GDGTs. *Geochim. Cosmochim. Acta*, *77*, 561–581.

910 Weber, Y., De Jonge, C., Rijpstra, W., Hopmans, E. C., Stadnitskaia, A.,
911 Schubert, C. J., Lehmann, M. F., Sinninghe Damsté, J. S., & Niemann, H.
912 (2015). Identification and carbon isotope composition of a novel branched
913 GDGT isomer in lake sediments: Evidence for lacustrine branched GDGT
914 production. *Geochim. Cosmochim. Acta*, *154*, 118–129.

915 Weber, Y., Sinninghe Damsté, J. S., Zopfi, J., De Jonge, C., Gilli, A., Schubert,
916 C. J., Lepori, F., Lehmann, M. F., & Niemann, H. (2018). Redox-dependent
917 niche differentiation provides evidence for multiple bacterial sources of glyc-
918 erol tetraether lipids in lakes. *Proc. Natl. Acad. Sci. U.S.A*, *115*, 10926–10931.

Weijers, J. W., Bernhardt, B., Peterse, F., Werne, J. P., Dungait, J. A., Schouten, S., & Damsté, J. S. S. (2011). Absence of seasonal patterns in mbt–cbt indices in mid-latitude soils. *Geochimica et Cosmochimica Acta*, *75*, 3179–3190.

Weijers, J. W., Panoto, E., van Bleijswijk, J., Schouten, S., Rijpstra, W. I. C., Balk, M., Stams, A. J., & Sinninghe Damsté, J. S. (2009). Constraints on the biological source (s) of the orphan branched tetraether membrane lipids. *Geomicrobiol. J.*, *26*, 402–414.

Weijers, J. W., Schouten, S., van den Donker, J. C., Hopmans, E. C., & Sinninghe Damsté, J. S. (2007). Environmental controls on bacterial tetraether membrane lipid distribution in soils. *Geochim. Cosmochim. Acta*, *71*, 703–713.

Weijers, J. W., Schouten, S., Hopmans, E. C., Geenevasen, J. A., David, O. R., Coleman, J. M., Pancost, R. D., & Sinninghe Damsté, J. S. (2006). Membrane lipids of mesophilic anaerobic bacteria thriving in peats have typical archaeal traits. *Environ. Microbiol.*, *8*, 648–657.

Xiao, W., Wang, Y., Zhou, S., Hu, L., Yang, H., & Xu, Y. (2016). Ubiquitous production of branched glycerol dialkyl glycerol tetraethers (brGDGTs) in global marine environments: a new source indicator for brGDGTs. *Biogeosciences*, *13*, 5883–5894.

Xiao, W., Xu, Y., Ding, S., Wang, Y., Zhang, X., Yang, H., Wang, G., & Hou, J. (2015). Global calibration of a novel, branched GDGT-based soil pH proxy. *Org. Geochem.*, *89*, 56–60.

Zell, C., Kim, J.-H., Moreira-Turcq, P., Abril, G., Hopmans, E. C., Bonnet, M.-P., Sobrinho, R. L., & Sinninghe Damsté, J. S. (2013). Disentangling the origins of branched tetraether lipids and crenarchaeol in the lower Amazon River: Implications for GDGT-based proxies. *Limnol. Oceanogr.*, *58*, 343–353.

947 Zhou, H., Hu, J., Spiro, B., Tang, J. et al. (2014). Glycerol dialkyl glycerol
948 tetraethers in surficial coastal and open marine sediments around China: In-
949 dicators of sea surface temperature and effects of their sources. *Palaeogeogr.*
950 *Palaeoclimatol. Palaeoecol.*, *395*, 114–121.

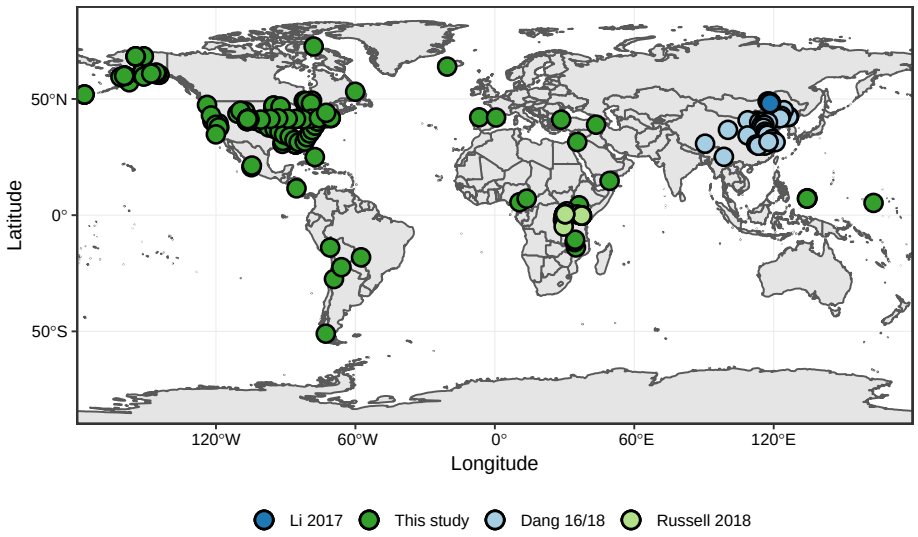

Figure 1: World map showing the location of the samples included in this dataset. Samples are color coded based to their source. Dark green points represent samples from our dataset; light green points are samples derived from Russell et al. (2018). Light blue samples represent sites included in Dang et al. (2018) and Dang et al. (2016a). Dark blue samples are from Li et al. (2017).

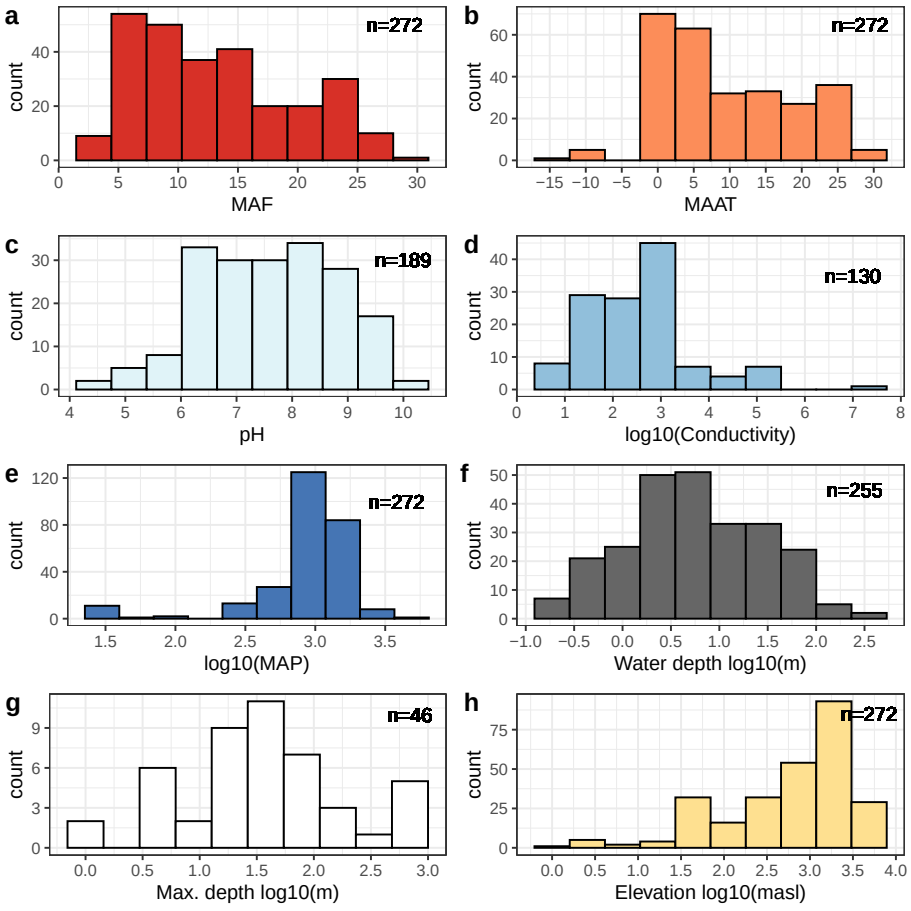

Figure 2: Distribution of environmental parameters in the dataset, number of samples with available data shown on top right. a) Mean Temperature of Months Above Freezing (MAF), b) Mean Annual Air Temperature (MAAT), c) pH, d) Conductivity (in log_{10}-transformed $\mu S/cm$), e) Mean annual precipitation (MAP, in log_{10}-transformed mm/month), f) Water Depth (in log_{10}-transformed m), g) Maximum depth of the lake (in log_{10}-transformed m), and h) Elevation (in log_{10}-transformed m.a.s.l.).

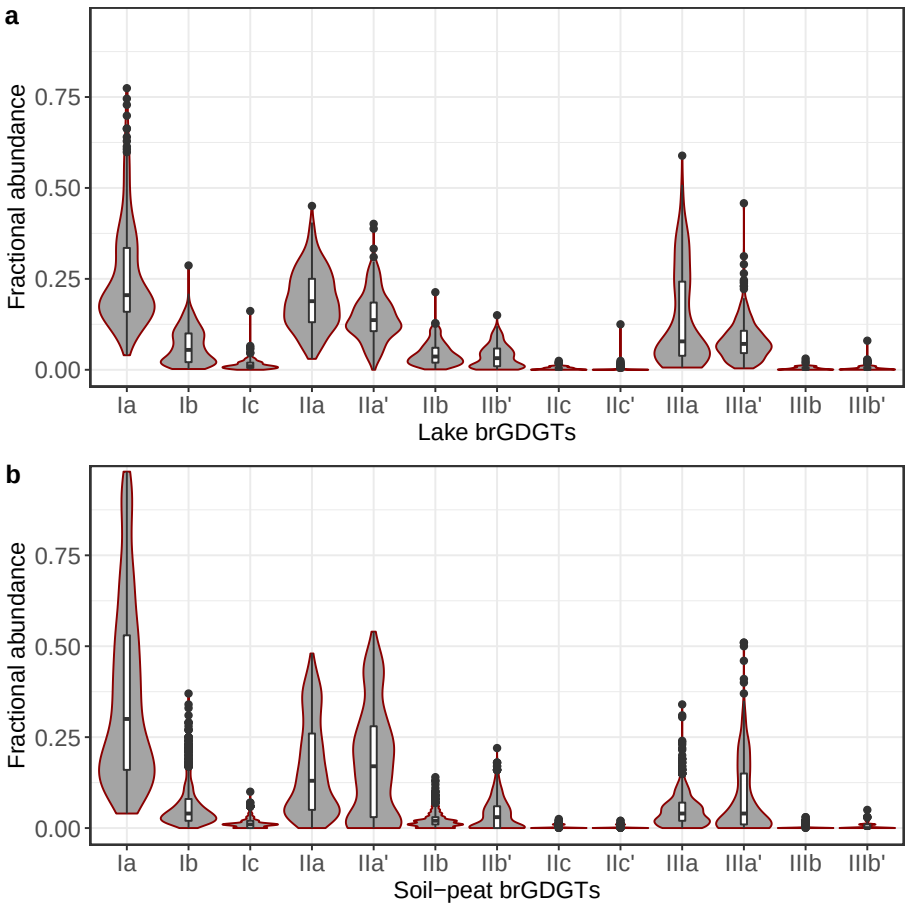

Figure 3: Distribution of each brGDGT in the a) lake and b) soil-peat datasets. Gray area of the violin plot shows the normalized distribution of the fractional abundance of each brGDGT. The mean value (horizontal black lines) for each structure is shown in the white boxplot inside each violin plot. Minor compounds $IIIc$ and $IIIc'$ are omitted.

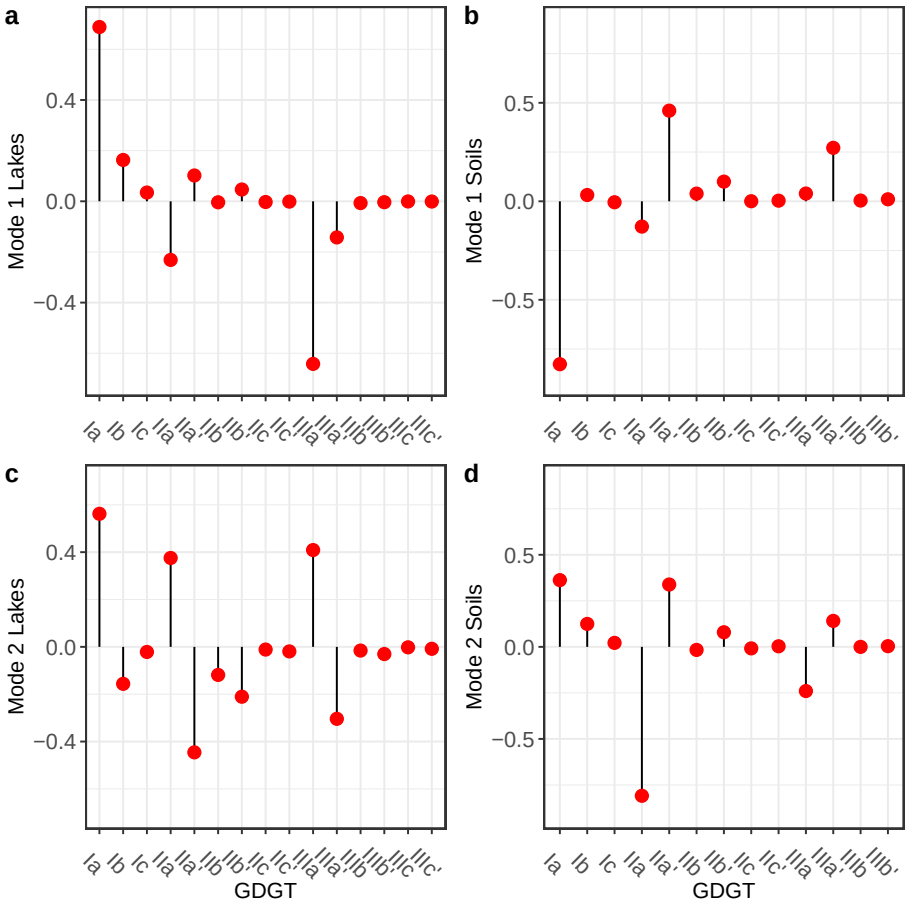

Figure 4: EOF loadings calculated for the lake (a and c) and soil-peat (b and d) datasets for Mode 1 (a and b), and Mode 2 (c and d).

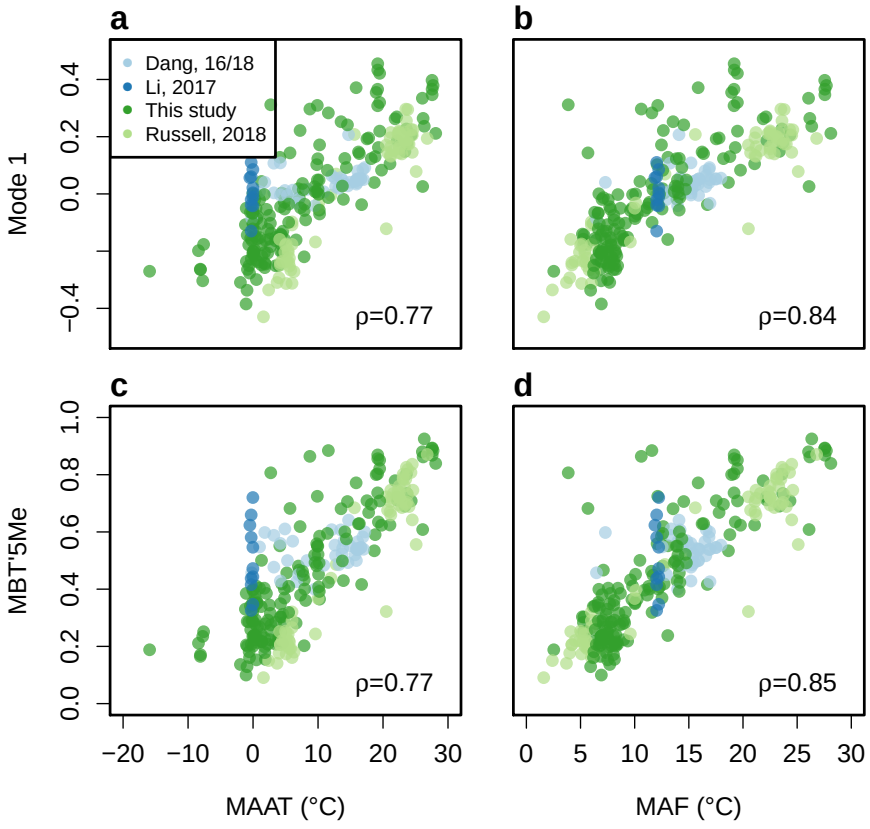

Figure 5: Scatter plots of Mean Annual Air Temperature (MAAT) (a and c), and Mean Temperature of Months Above Freezing, MAF, (b and d) against values for Mode 1 (a and b) and MBT'_{5Me} (c and d). Spearman correlation values (ρ) are listed in the lower right hand corner. Samples are color coded following Figure 1.

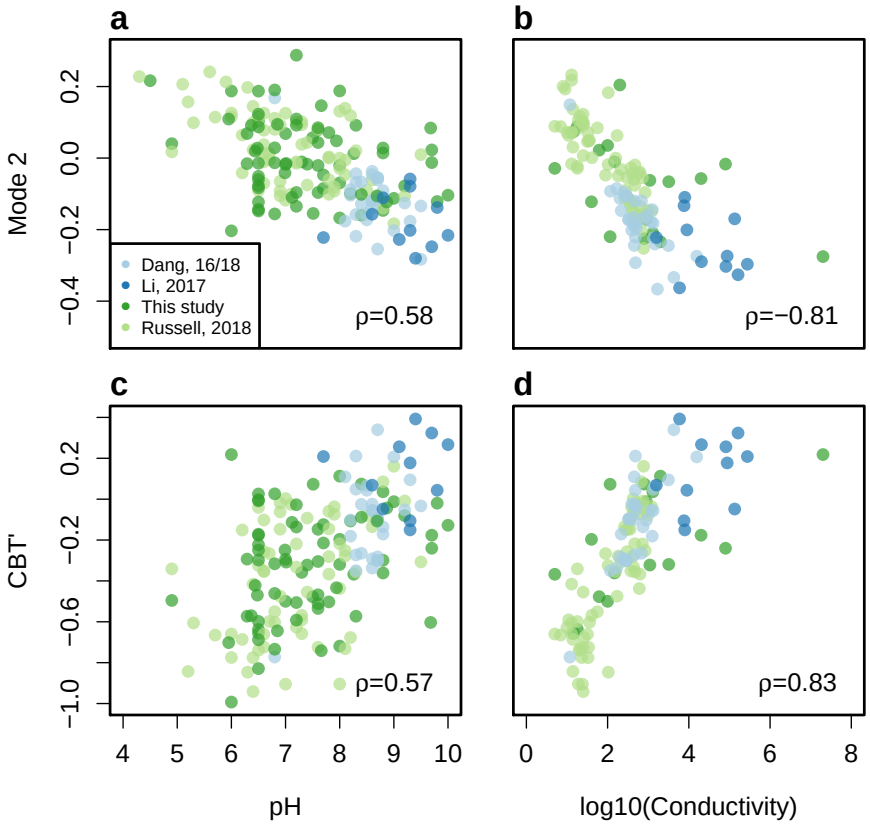

Figure 6: Scatter plots of pH (a and c), and log_{10}-transformed conductivity ($\mu S/cm$), (b and d) against values for Mode 2 (a and b), and CBT' (c and d). Spearman correlation values are presented for each plot. Samples are color coded following Figure 1.

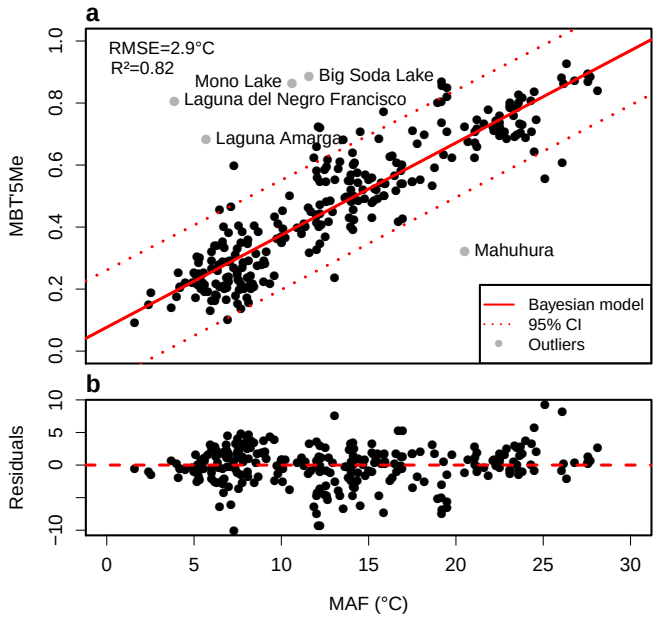

Figure 7: Bayesian regression calculated for MBT'_{5Me} as a function of Mean Temperature of Months Above Freezing (MAF). a) Scatter plot showing the regression with fitted line (solid red) and the 95% Confidence Interval (dotted red) for the dataset without outliers (labeled and shown in grey). Calculated R^2 and RMSE values for the regression are indicated in the corner. b) Residuals plotted against MAF.

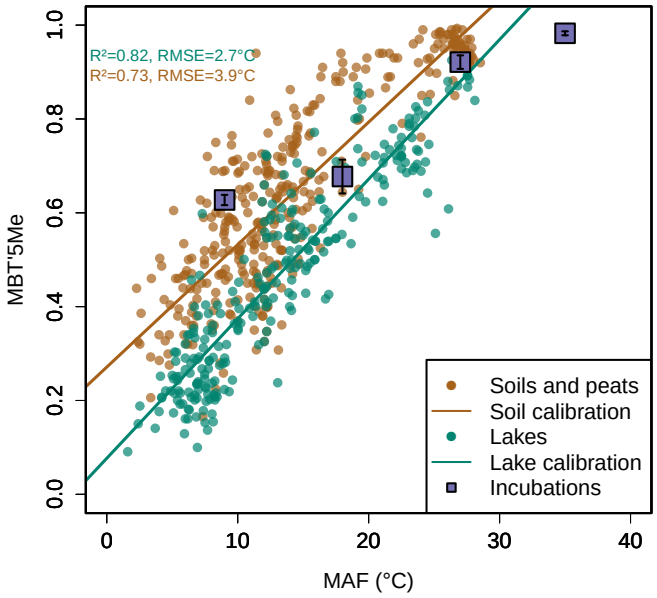

Figure 8: Scatter plot of MBT'_{5Me} as a function of Mean Temperature of Months Above Freezing (MAF) for soils and peats (brown, Dearing Crampton-Flood et al. (2020) and Li et al. (2017)), lakes (green, this study), and temperature incubations from Martínez-Sosa et al. (2020) (outlined purple squares). R^2 and RMSE values for each calibration line are listed in the upper left hand corner. Standard deviations for the incubation results are shown as error bars.

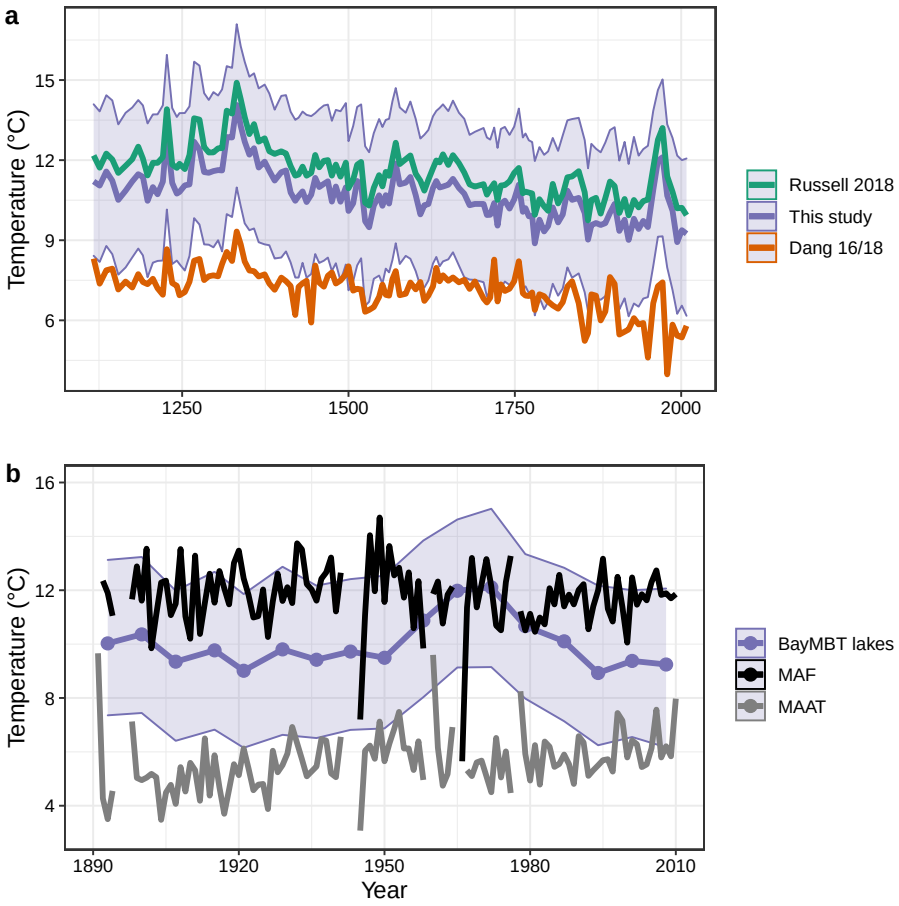

Figure 9: Temperature reconstruction for the Basin Pond record (Miller et al., 2018). a) Reconstructions using the Russell et al. (2018), Dang et al. (2018), and the Bayesian calibration from this work are shown in green, orange and purple, respectively. Purple shaded area indicate the 1σ error range for the Bayesian results. All 180 data points presented without any processing. b) BayMBT median results (purple) with the 1σ bounds (shaded purple area) compared with the instrumental record (1891–2019) from Farmington, ME. Record for Mean Annual Air Temperature (MAAT) is shown as a gray line, Mean Temperature of Months Above Freezing (MAF) is shown as a black line.

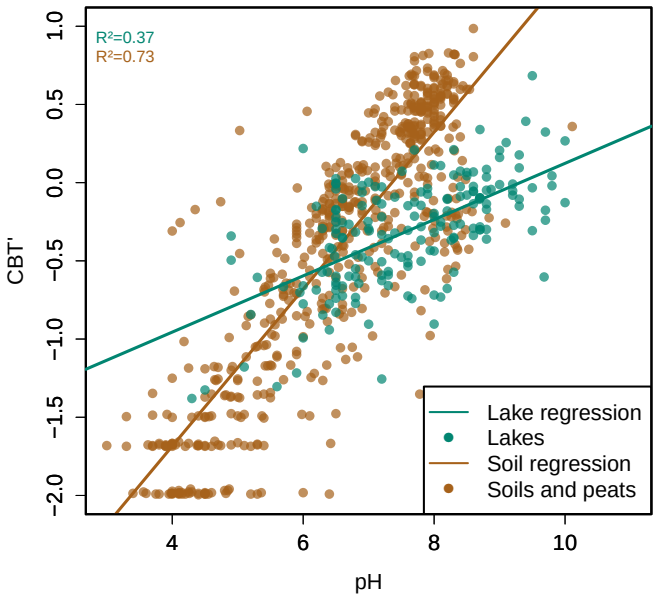

Figure 10: Scatter plot and linear regressions of CBT' as a function of pH for soil and peat samples (brown, Dearing Crampton-Flood et al. (2020) and Li et al. (2017)) and lakes (green, this study). R^2 values for each regression are shown on top left.

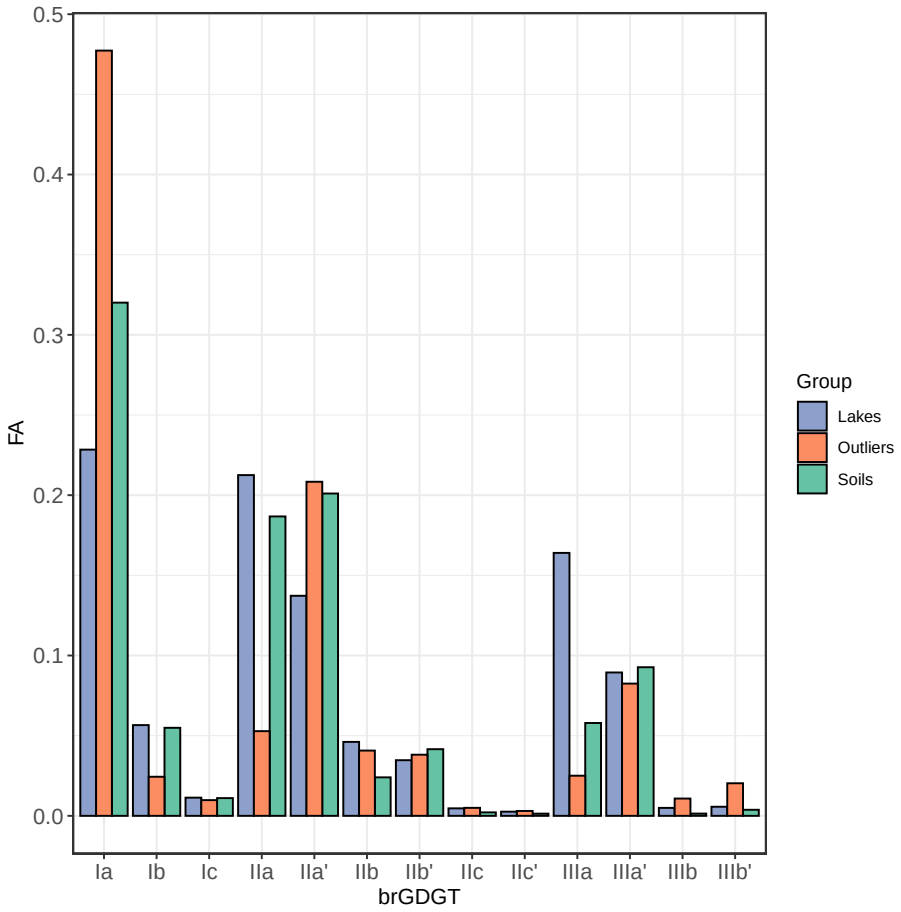

Figure 11: Comparison of the mean fractional abundance (FA) of the saline, alkaline outlier lakes (orange) with lake (blue) and soil and peats (green) in the same temperature range (3−21°C). Error bars show the standard deviation of the data in each group.

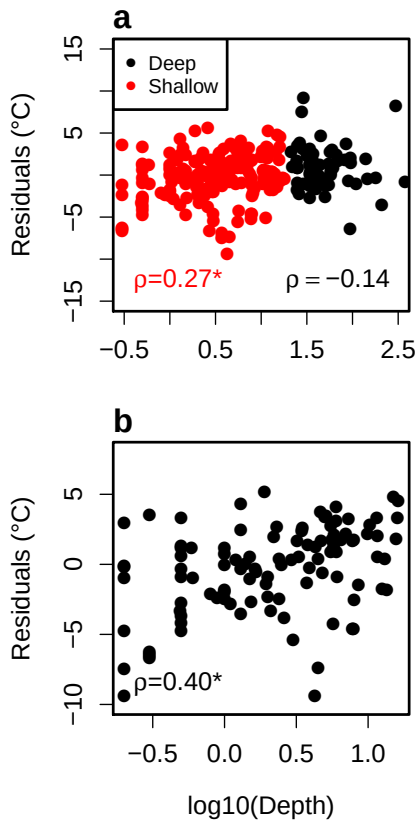

Figure 12: Scatter plots and correlations of the calibration residuals as a function of the log_{10}-transformed depth (m). a) Lakes are separated into shallow (red, < 20 m) and deep (black, > 20 m) groups. The Spearman correlation for each subset is shown; asterisks mark significant correlations ($p < 0.05$). b) Shallow lakes from temperate latitudes ($> 35°$N and S). Spearman correlation is shown.

Parameters	Correlation
MAF - pH	0.33*
MAF - MAP	-0.21*
MAF - Depth	0.08
MAF - Conductivity	0.43*
MAF - Elevation	-0.48*
pH - MAP	-0.48*
pH - Depth	-0.21*
pH - Conductivity	0.67*
pH - Elevation	-0.26*
MAP - Depth	0.21*
MAP - Conductivity	-0.83*
MAP - Elevation	0.21*
Conductivity - Depth	-0.17
Conductivity - Elevation	-0.56*
Depth - Elevation	0.31*

Table 1: Spearman correlation values for each pair of environmental parameters considered in our dataset. Statistically significant correlations ($\rho < 0.05$) are marked with an *.

Parameter	Mode 1 (L)	Mode 2 (L)	Mode 1 (S)	Mode 2 (S)
MAF	0.84*	-0.28*	-0.27*	0.68*
MAAT	0.77*	-0.07	-0.42*	0.56*
pH	0.29*	-0.58*	0.73*	0.40*
MAP	-0.01	0.58*	-	-
Conductivity	0.39*	-0.81*	-	-
Depth	-0.14*	0.01	-	-
Elevation	-0.45*	0.14*	-	-

Table 2: Spearman correlation values for both Modes (Lakes and Soils, L and S respectively) and all studied environmental parameters. Statistically significant correlations ($\rho < 0.05$) are marked with an *.

Index	MAF	MAAT	pH	MAP	Conductivity	Depth	Elevation
MBT'_{5Me}	0.85*	0.77*	0.33*	-0.05	0.48*	-0.10	-0.44*
MBT'_{6Me}	0.39*	0.56*	-0.23*	0.44*	-0.45*	-0.01	-0.01
CBT'	0.34*	0.11	0.57*	-0.59*	0.83*	0.08	-0.14*
IR	0.61*	0.41*	0.53*	-0.46*	0.77*	-0.05	-0.23*
fC	0.64*	0.57*	0.42*	-0.20*	0.44*	-0.11	-0.40*

Table 3: Spearman correlation values for calculated indices and environmental parameters. Statistically significant correlations ($\rho < 0.05$) are marked with an *.